Comput Mech (2013) 52:971–981
DOI 10.1007/s00466-013-0858-3

ORIGINAL PAPER

Fluid–structure interaction simulation of pulsatile ventricular assist devices

C. C. Long · A. L. Marsden · Y. Bazilevs

Received: 20 December 2012 / Accepted: 30 March 2013 / Published online: 18 April 2013

Abstract In this paper we present a collection of fluid–structure interaction (FSI) computational techniques that enable realistic simulation of pulsatile Ventricular Assist Devices (VADs). The simulations involve dynamic interaction of air, blood, and a thin membrane separating the two fluids. The computational challenges addressed in this work include large, buckling motions of the membrane, the need for periodic remeshing of the fluid mechanics domain, and the necessity to employ tightly coupled FSI solution strategies due to the very strong added mass effect present in the problem. FSI simulation of a pulsatile VAD at realistic operating conditions is presented for the first time. The FSI methods prove to be robust, and may be employed in the assessment of current, and the development of future, pulsatile VAD designs.

Keywords Pulsatile VAD · Fluid–structure interaction · Isogeometric analysis · Biomechanics · Finite elements · Blood flow · Rotation-free shells

1 Introduction

Ventricular Assist Devices (VADs) are devices which provide mechanical circulatory support to a single ventricle of the heart [33,4]. They are used primarily as a bridge to transplant, extending the life of the patient until a compatible donor can be found. Two device types are available: pulsatile displacement pump designs, and a continuous flow impeller designs. Devices now available to the pediatric community include only pulsatile designs, and the we therefore choose to focus on pulsatile VADs in this work. The pediatric population suffers from increased risk of thromboembolic events (i.e., blood clots) while using VADs, and thrombo-embolic events may occur in up to 40 % [5] of cases. This has made these devices too risky for long-term use, and reliable only as a short-term bridge to transplant. However, in children, particularly those with congenital heart defects or cardiomyopathy, it may be of particular importance to develop a long-term reliable device. Pediatric patients in heart failure due to dilated cardiomyopathies have shown recovery of the native heart tissue when a VAD is used in a bridge to recovery scenario. This is an effect that has not been observed in the adult population [23].

A pulsatile VAD provides mechanical support to a single ventricle of the heart. A patient may receive two VADs if support is required for both ventricles, depending on the underlying disease state. The design of the device is as follows: Two domed chambers are separated by a flexible polyurethane membrane. One chamber is an air compartment, which is driven pneumatically. The other is a blood chamber, which delivers blood from the right atrium/left ventricle to the pulmonary arteries/aorta, for a Right/Left heart VAD, respectively [4]. The flow in the air chamber moves the thin membrane, which causes displacement in the blood chamber and drives the blood through the device.

The low survival rates of VADs may be alleviated if one had a better understanding of how specific flow features in the blood chamber are linked to the formation of blood clots. For this, as a first step, one needs the ability to accurately predict the blood flow itself inside the device. The latter is not possible without fluid–structure interaction (FSI) modeling

Y. Bazilevs (✉)
University of California, San Diego, 9500 Gilman Drive,
Mail Code 0085, La Jolla, San Diego, CA 92093-0085, USA
e-mail: yuri@ucsd.edu

C. C. Long · A. L. Marsden
University of California, San Diego, 9500 Gilman Drive,
Mail Code 0411, La Jolla, San Diego, CA 92093-0085, USA

that involves the interaction of air, blood, and a thin membrane separating the two fluids. For the modeling to be realistic, the relatively complex geometry of the VAD, the large, time-dependent motions of the membrane, and the actual pump operating conditions (i.e., flow rates and pressures) must be taken into account. In this work we present computational FSI methods in which these effects are incorporated, and which may be used for high-fidelity VAD design. While there is extensive literature on patient specific modeling for pediatric applications with and without FSI [52,31,53], very little has been done to date for numerical simulation of pulsatile VADs. In [30] an idealized VAD design was analyzed with a linearly elastic shell model for the membrane and non-physiological outlet boundary conditions, and in [50] VAD simulations were performed using imposed membrane motion rather than true FSI. We stress that membrane motion in a VAD is expected to be critical to the device's performance, and thus accurate prediction of the time-dependent membrane response is crucial to the simulation and design of the device. To the best of the authors' knowledge this is the first 3D, full-scale, high-fidelity FSI modeling of pulsatile VADs.

The paper is outlined as follows. In Sect. 2, we present the computational methods employed to simulate the VAD–FSI problem. A rotation-free isogeometric Kirchhoff–Love shell formulation is used to model the thin membrane in combination with a moving-domain ALE–VMS finite element formulation for the blood and air flow. The FSI solution strategy involves strong coupling, which is accomplished using a combination of sparse-matrix-based and matrix-free techniques. Strong coupling is essential for convergence of the coupled FSI equation system for this application. In Sect. 3 we provide a detailed description of the VAD problem setup and present a numerical simulation of the device. In the course of the simulation we periodically remesh the fluid mechanics domain to maintain good quality of the finite element discretization. The simulation predicts physiologically realistic blood flow features and membrane deformation patterns. In Sect. 4 we draw conclusions and present future research directions.

2 Numerical methods for VAD–FSI

In this section we briefly discuss the fluid and structural mechanics formulations used in this work, namely ALE–VMS and Isogeometric Analysis (IGA), respectively. We mostly summarize the main features of these methods and provide references where the reader may find the mathematical details of these techniques. One of the main computational challenges of this work is robust FSI coupling, which we present in some detail in this section

2.1 ALE–VMS fluid mechanics formulation

Standard Galerkin methods are not a sufficiently robust technology for advection-dominated flows. For this reason, stabilized methods [22,43,87,39,78,85,86,80,42,88, 37] were designed to circumvent this shortcoming of the Galerkin technique. Stabilized methods, which are essentially residual-based modifications of the Galerkin method, exhibit uniform stability and convergence behavior across the full range of advective and diffusive phenomena.

The basic theory of variational multiscale (VMS) methods was developed in [38], wherein stabilized methods were first identified as multiscale methods. Relationship between stabilized methods and subgrid scale modeling was also identified in [38], and now presents an important research direction [41]. Recently, in [7], the authors proposed a residual-based turbulence modeling and computational framework that is based on the VMS theory, named RBVMS. This technique performs well on both laminar and turbulent flows, for a wide range of Reynolds numbers.

The extension of the RBVMS framework to the moving-domain case, where the motion of the fluid mechanics domain is handled using the Arbitrary Lagrangian–Eulerian (ALE) formulation [40], was named ALE–VMS in [69,14]. The ALE–VMS formulation discretized with linear tetrahedral FEM is used in this work to compute the fluid mechanics part of the VAD problem.

An important additional feature of the ALE–VMS methodology is weak enforcement of essential boundary conditions. Weakly enforced essential boundary conditions were introduced in [15] in order to improve solution accuracy on meshes with insufficient boundary-layer resolution [16,17, 6,34]. Although the weak BCs are now routinely used for wind-turbine aerodynamics [13,35,36] and ship hydrodynamics [2,1,3], we do not use them in this work. However, we feel that they will likely be beneficial in cardiovascular blood flow and FSI computations in that they may further improve boundary-layer accuracy and produce more accurate wall quantities such as wall shear stress or oscillating shear index, which are critically important in numerous cardiovascular applications [65,68,99,100,71–73,10,96,74,70,69,52].

2.2 Rotation-free isogeometric thin shell formulation

The circular membrane separating the blood and air chambers of the device is a very thin structure. The membrane stress-free reference configuration is not flat, but convex. As the membrane undergoes large cyclic deformation, it is almost always in a state of compression, which leads to local buckling and wrinkling. As a result, it is desirable to represent the membrane or thin shell with numerical technology that is efficient and capable of representing the underlying complex structural dynamics without posing significant challenges associated with robustness of the structural mechanics computations and large local deformations of the fluid mechanics domain boundary.

Low-order, bi-linear quadrilateral finite elements, which are widely used and are considered standard shell element technology, exhibit several shortcomings: (1) These elements require the use of displacement and rotation degrees of freedom to describe shell kinematics; (2) One needs a fine mesh to represent shell geometries with high local curvature, and to simultaneously achieve the desired solution accuracy; (3) Ad-hoc element technology is necessary to overcome membrane and shear locking; (4) In the case of implicit time integration employed in this work, the presence of rotational degrees of freedom doubles the size of the solution and right-hand-side residual arrays, quadruples the size of the left-hand-side matrix, and results in an order-of-magnitude increase in linear solver time.

Isogeometric shell analysis was recently proposed in [20] to address the shortcomings of standard shell technology listed above. It was found that higher-order continuity (C^1 and above) of the IGA basis functions significantly improved the per-degree-of-freedom accuracy and robustness of thin shell discretizations as compared to the FEM. Furthermore, the increased continuity of the IGA discretizations enabled the use of shell kinematics without rotational degrees of freedom [49,19,21], leading to further computational cost savings. The isogeometric rotation-free Kirchhoff–Love shell formulation for structures composed of multiple structural patches, called the bending strip method, was developed in [48], which enabled the application of the rotation-free IGA technology to real-life structures, such as wind turbine rotors (see [12,11,36]). Besides significant savings in computational time, the rotation-free shell discretization makes FSI coupling simpler than the discretization with rotational degrees-of-freedom. Finally, the smooth structural motion computed with IGA gives a smooth fluid mechanics mesh at the fluid–structure boundary, which adds accuracy and robustness to the fluid mechanics computation.

Non-uniform rational B-splines (NURBS) [61] are employed in this work to discretize the structural mechanics equations of the membrane separating the blood and air chambers. T-splines [8,28], a relative newcomer to IGA currently receiving significant attention, are also well suited for the proposed structural modeling approach. For related rotation-free shell formulations the reader is also referred to [26,25,27,60,59,57].

2.3 FSI coupling

In order to take advantage of the benefits of IGA for structural mechanics, and to leverage the existing advanced automatic mesh generation tools for the FEM, we choose to couple low-order FEM for the fluid and IGA for structural mechanics. As a result, the FSI coupling assumes a nonmatching fluid–structure interface discretization. Nonmatching interface discretizations in FSI problems necessitate the use of interpolation or projection of kinematic and traction data between the nonmatching surface meshes (see, e.g., [32,88,92,95,71, 97,98,73,74,96,69,13,76,18], where [76] is more comprehensive than [74]). A computational procedure, which can simultaneously handle the data transfer for IGA and FEM discretizations, was proposed in [13]. The procedure also includes a robust approach in identifying “closest points” for arbitrary shaped surfaces. While such interface projections are rather straightforward for loosely-coupled FSI algorithms, they require special techniques (such as developed in [88,89,93,95,71,72,75,76,18] as well as this paper) for strongly-coupled methods that are monolithic-like and that are necessary for the present application.

A full discretization of the FSI formulation leads to coupled, nonlinear equation systems that need to be solved at every time step.The equation systems can be written as follows:

$$\mathbf{N}_1\left(\mathbf{d}_1, \mathbf{d}_2, \mathbf{d}_3\right) = \mathbf{0}, \tag{1}$$

$$\mathbf{N}_2\left(\mathbf{d}_1, \mathbf{d}_2, \mathbf{d}_3\right) = \mathbf{0}, \tag{2}$$

$$\mathbf{N}_3\left(\mathbf{d}_1, \mathbf{d}_2, \mathbf{d}_3\right) = \mathbf{0}. \tag{3}$$

Here $\mathbf{N}_1$, $\mathbf{N}_2$, and $\mathbf{N}_3$ are the discrete residual functions, and $\mathbf{d}_1$, $\mathbf{d}_2$, and $\mathbf{d}_3$ are the vectors of nodal (or control-point in the case of IGA) unknowns, corresponding to the fluid mechanics, structural mechanics, and mesh problems,

In the block-iterative coupling [82,84,56,47,90,91,94, 81,88,18], the fluid, structure, and mesh systems are treated as separate blocks, and the nonlinear iterations are carried out sequentially. First, the fluid block is solved, then the structure, and then the mesh. In solving a given block of equations the most current values of the other blocks of unknowns are used. The sequence of solves is repeated until all the equation systems are solved to an a priori set tolerance. This strategy is the easiest to implement, and it performs very well in applications where the structure is heavy relative to the surrounding fluid.

In the present application, the membrane separating the blood and air chambers of the VAD is extremely thin, and its mass is significantly smaller than the mass of the surrounding fluid that is displaced as a result if the membrane motion. Because of the relatively low structural mass, block-iterative FSI is not an appropriate technique for this application. Instead, we employ the quasi-direct coupling technique [90,91,94,88,18], where the fluid+structure and mesh systems are treated as two separate blocks, and the nonlinear iterations are carried out one block at a time until all the equation systems are solved to an a priori set tolerance. In an iteration step, given the solution at i, the solution

$i + 1$ is obtained by solving the following two blocks of equations:

$$\left.\frac{\partial \mathbf{N}_1}{\partial \mathbf{d}_1}\right|_i \Delta \mathbf{d}_1^i + \left.\frac{\partial \mathbf{N}_1}{\partial \mathbf{d}_2}\right|_i \Delta \mathbf{d}_2^i = -\mathbf{N}_1\left(\mathbf{d}_1^i,\ \mathbf{d}_2^i,\ \mathbf{d}_3^i\right), \tag{4}$$

$$\left.\frac{\partial \mathbf{N}_2}{\partial \mathbf{d}_1}\right|_i \Delta \mathbf{d}_1^i + \left.\frac{\partial \mathbf{N}_2}{\partial \mathbf{d}_2}\right|_i \Delta \mathbf{d}_2^i = -\mathbf{N}_2\left(\mathbf{d}_1^i,\ \mathbf{d}_2^i,\ \mathbf{d}_3^i\right), \tag{5}$$

$$\mathbf{d}_1^{i+1} = \mathbf{d}_1^i + \Delta \mathbf{d}_1^i, \tag{6}$$

$$\mathbf{d}_2^{i+1} = \mathbf{d}_2^i + \Delta \mathbf{d}_2^i, \tag{7}$$

$$\left.\frac{\partial \mathbf{N}_3}{\partial \mathbf{d}_3}\right|_i \Delta \mathbf{d}_3^i = -\mathbf{N}_3\left(\mathbf{d}_1^{i+1},\ \mathbf{d}_2^{i+1},\ \mathbf{d}_3^i\right), \tag{8}$$

$$\mathbf{d}_3^{i+1} = \mathbf{d}_3^i + \Delta \mathbf{d}_3^i. \tag{9}$$

The above systems of linear equations are solved using a GMRES technique [63], requiring the computation of matrix-vector products. In this work the matrix-vector products involving $\left.\frac{\partial \mathbf{N}_1}{\partial \mathbf{d}_1}\right|_i$, $\left.\frac{\partial \mathbf{N}_2}{\partial \mathbf{d}_2}\right|_i$, and $\left.\frac{\partial \mathbf{N}_3}{\partial \mathbf{d}_3}\right|_i$ are computed using a sparse-matrix-based approach, where the tangent matrices are derived analytically and assembled into a sparse-matrix data structure in a standard fashion. The remaining matrix-vector products involving $\left.\frac{\partial \mathbf{N}_1}{\partial \mathbf{d}_2}\right|_i$ and $\left.\frac{\partial \mathbf{N}_2}{\partial \mathbf{d}_1}\right|_i$ are approximated using a matrix-free approach, namely

$$\left.\frac{\partial \mathbf{N}_1}{\partial \mathbf{d}_2}\right|_i \Delta \mathbf{d}_2^i = \frac{\mathbf{N}_1\left(\mathbf{d}_1^i,\ \mathbf{d}_2^i+\epsilon_1\Delta\mathbf{d}_2^i,\ \mathbf{d}_3^i\right)-\mathbf{N}_1\left(\mathbf{d}_1^i,\ \mathbf{d}_2^i,\ \mathbf{d}_3^i\right)}{\epsilon_1}, \tag{10}$$

$$\left.\frac{\partial \mathbf{N}_2}{\partial \mathbf{d}_1}\right|_i \Delta \mathbf{d}_1^i = \frac{\mathbf{N}_2\left(\mathbf{d}_1^i+\epsilon_2\Delta\mathbf{d}_1^i,\ \mathbf{d}_2^i,\ \mathbf{d}_3^i\right)-\mathbf{N}_2\left(\mathbf{d}_1^i,\ \mathbf{d}_2^i,\ \mathbf{d}_3^i\right)}{\epsilon_2}, \tag{11}$$

where ϵ_1 and ϵ_2 are relatively small real numbers. This mixed analytical/numerical, matrix-based/vector-based approach was proposed for coupled problems in general in [79], and for FSI problems specifically in [88], where the numerical, vector-based computation is applied to the computation with the $\left.\frac{\partial \mathbf{N}_1}{\partial \mathbf{d}_3}\right|_i$ block.

We feel the proposed approach is well suited for cases that require a relatively larger number of GMRES iterations ($O(100)$) for good overall nonlinear convergence. This is because the sparse matrices are formed once every nonlinear iteration (or, possibly, once every time step to further decrease the computational cost), making the associated computational cost independent of the number of GMRES iterations employed. Although matrix-vector products given by Eqs. (10) and (11) need to be performed once per GMRES iteration, the FEM assembly takes place over a narrow band of fluid elements near the fluid–structure interface, which is a lot less expensive than assembling the discrete residuals over the entire fluid mechanics domain. For a comprehensive exposition of sparse-matrix-based and matrix-free approaches see [18].

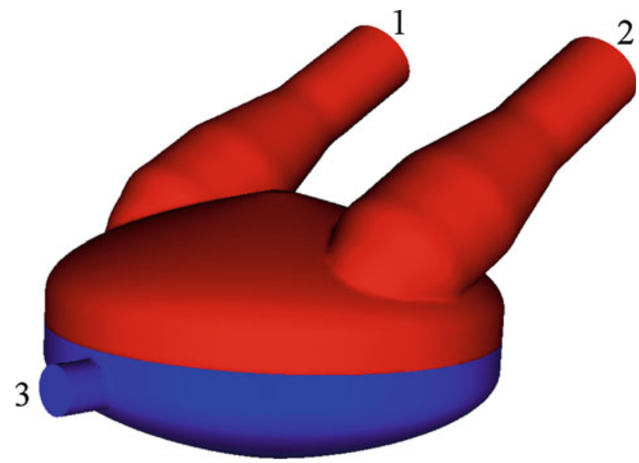

Fig. 1 The computational domain, with the blood domain in *red*, and the air domain in *blue*. The inlet and outlet face of the blood chamber are labeled 1 and 2, respectively. The air-side inlet/outlet face is labeled 3. (Color figure online)

3 VAD simulation

3.1 Problem setup

Geometry For the initial study, we use a generic VAD device as our computational domain. Geometric parameters, such as width, height, and angles of the entrance/exit arms are consistent with current designs, and are meant to be a generic representation of current commercially available devices. The chosen design for the initial study has a width of 7.7 cm, and an apex to apex height of 4.5 cm. The incline angle between the arms and the main blood chamber is 30°, with one assigned exclusively as the inlet, and the other as an outlet. The outlet faces are 1.5 cm in diameter. The air chamber has one small inlet/outlet port of diameter 0.8 cm. These are labeled in Fig. 1.

A stroke volume of 73 mL was chosen for this device, which yields an ejection fraction of 68 %. A beat frequency of 80 bpm is used, for a pump output of 5.8 L/min. This initial study uses a VAD that is too large to be considered a pediatric model, but all data is within an acceptable physiologic range for adult models.

Boundary conditions Each pump cycle may be broken up into two components: the fill stage and the ejection stage. We impose the fill period of 0.45 s, and the ejection period of 0.3 s, and we also enforce that each stage must fill or eject the same volume, 73 mL. For simplicity, the flow is assumed to behave sinusoidally during each stage. We can therefore impose the air chamber inflow flow rate q at a given time t as

$$q = \begin{cases} q_e \sin^{\frac{1}{2}}\left(\frac{t}{0.3}\pi\right) & \text{if } t < 0.3 \\ q_f \sin^{\frac{1}{2}}\left(\frac{t-0.3}{0.45}\pi\right) & \text{otherwise} \end{cases}, \tag{12}$$

where q_e and q_f are constants equal to the peak flow rate of each stage. The constants may be obtained from the equations

$$\int_0^{0.3} q_e \sin^{\frac{1}{2}}\left(\frac{t}{0.3}\pi\right) \mathrm{d}t = 73, \tag{13}$$

and

$$\int_{0.3}^{0.75} q_f \sin^{\frac{1}{2}}\left(\frac{t-0.3}{0.45}\pi\right) \mathrm{d}t = -73, \tag{14}$$

and are equal to $q_e = 319.02$ cc/s and $q_f = -212.68$ cc/s.

On the blood side, we alternate boundary conditions at the inlet/outlet between a Neumann condition and a Dirichlet condition as necessary since we do not directly compute the valve motion in the simulation. At the outlet, for example, we have two conditions. If we are in the fill stage, then we impose a zero-velocity (i.e., no flow) boundary condition. During the ejection, however, we impose a resistance boundary condition

$$p = C_r q + p_0,$$

where q is the volumetric flow rate on the outlet face, C_r is a prescribed resistance value, p_0 is the distal pressure, and p is the pressure at the outlet face. For the simulation we choose p_0 to be 65 mmHg, which enforces a minimum pressure of 65 mmHg during the expel. The resistance value is set to $C_r = 183$ g/(s cm^4), which gives a maximum systolic pressure of 108 mmHg. The inlet face uses the same boundary conditions, but, obviously, with opposite phase.

The structural membrane is simply supported around the circumference.

Remark Note that, because the incompressible flow assumption is employed for both blood and air, the flow rate into the air chamber must equal to the flow rate out of the blood chamber, and vice versa. As a result, by controlling the total volume of the air going in and out of the air chamber, we automatically control the total volume of the blood flowing in and out of the blood chamber. The proposed quasi-direct FSI coupling guarantees that at every nonlinear iteration this balance holds. Loosely-coupled FSI approaches, besides being unsuitable for this problem due to the strong added mass effect, cannot guarantee this balance unless special procedures are devised to enforce it (see, e.g., [51]).

Blood, air, and membrane properties Both air and blood are treated as incompressible, Newtonian fluids. The blood density and dynamic viscosity are set to 1 g/cm^3 and 0.04 poise, respectively. The air density and dynamic viscosity are set to 1.205×10^{-3} g/cm^3 and 2×10^{-4} poise, respectively. Given the VAD geometry, fluid properties, and flow rates employed, the peak Reynolds number is about 10,000 in the blood chamber, and 7,000 in the air chamber. These values are based on the inlet/outlet branch diameters and flow speeds. Note that the VAD blood chamber Reynolds number, which is higher than that in the large blood vessels of the human cardiovascular system (e.g., the thoracic aorta), is in the turbulent range.

The membrane is a flexible thin sheet, commonly made of polyurethane. We use membrane material properties consistent with those of the Penn State VAD, the LionHeart [29]. The LionHeart membrane has a thickness of 0.38 mm, density of 1.1 g/cm^3, and Young's modulus of 550 MPa [29]. In our simulation, we use a thinner membrane of 0.25 mm, which is reflective of the smaller device used for the pediatric population, as was provided in a private communication from the authors of [62]. The membrane initial configuration is obtained by taking a circular disc, which is exactly represented using a single NURBS patch with four corner singularities, and displacing the interior control points in the direction normal to the plane of the disc toward the air chamber. The initial shape of the membrane is assumed to be sinusoidal, and the control-point displacement d is given by the equation

$$d = 1.52 \cos\left(\frac{r}{3.85}\frac{\pi}{2}\right), \tag{15}$$

where r is the radial distance of the control point from the center of the disc.

Meshing, mesh moving, and remeshing The blood and air chamber volumes in the reference configuration are meshed using MeshSim automatic mesh generator (Symmetrix Inc., Clifton Park, NY). The number of elements in the air chamber is 238,322 and in the blood chamber is 497,160. The membrane is discretized using 1,024 C^1-continuous quadratic NURBS elements. The simulations are run for two time cycles of 0.75 s each, with a time step size of 1.0 ms. Generalized-α time integration is used for the coupled FSI equation system (see [24,44,9]).

As the computation proceeds, the fluid mechanics mesh is moved using equations of elastostatics with Jacobian-based stiffening [83,77,45,18], which better preserves the mesh quality in the simulations than the no-stiffening approach and delays the necessity to remesh. However, due to very large motions of the membrane the mesh eventually becomes highly deformed and a remesh is necessary to preserve the quality of the fluid mechanics discretization. The necessity to remesh is quantified in terms of the change in the element volume as measured by the ratio of the Jacobian determinants of the elements in the current step and the step immediately after the previous remesh. For this simulation, remeshing is performed once the ratio of 72 % for compression or 170 % for expansion is achieved.

During the remesh the surface meshes of the blood and air chamber, including those at the fluid–structure interface, are preserved, and a new tetrahedral mesh is generated on the interior of both subdomains. The solution data at the current step, which includes fluid velocity, acceleration, and

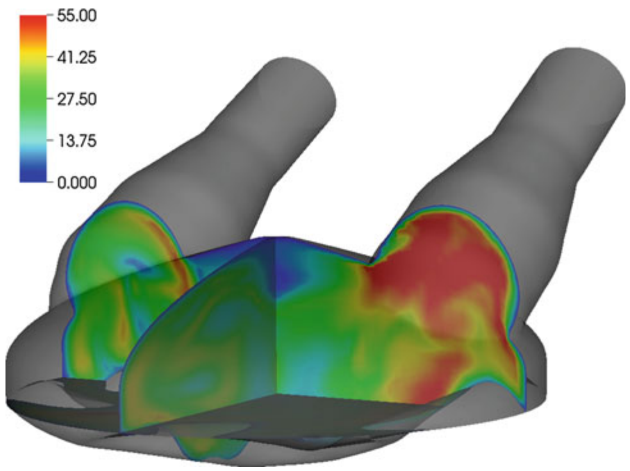

Fig. 2 Flow speed (cm/s) in the deformed blood chamber configuration at $t = 0.15$ s

Fig. 3 Top view of the membrane deformed configuration at $t = 0.15$ s. Despite the complex deformation pattern, the wrinkles on the membrane surface are smooth

pressure, as well as mesh velocity and displacement, is transferred to the new mesh by means of a nodal interpolation procedure that involves the computation of the inverse mapping. To efficiently locate the element in the old mesh containing the nodal point of interest, we use a "point in a polygon" method [58]. Once the data is transferred to the new mesh, the FSI computation continues. No special procedures for transferring the pressure data (e.g., pressure clipping [46,88,74]) are employed.

3.2 Simulation Results

The VAD simulation was carried out in a parallel computing environment at the San Diego Supercomputing Center [67]. The simulation was run for two time cycles. All the data presented is gathered from the second time cycle. The time $t = 0$ in all figures refers to the beginning of the second cycle.

Figures 2, 3, and 4 show snapshots of the computed blood flow speed and membrane deformation. The simulation captures a very complex membrane motion, with many folds, clearly seen in Figs. 3 and 4. The deformed membrane surface is notably smooth, with no sharp kinks on the mesh edges, which is due to the underlying smoothness of the NURBS discretization. This buckling motion is smoother than is typically attained using more traditional methods. Since the structural kinematics is used to drive the fluid mechanics mesh deformation, the smoother buckling motion ensures that the fluid mechanics mesh at the fluid–structure interface remains smooth.

During the fill stage, the inlet jet impinges on the chamber wall, and flows along the wall creating a strong vortex. The vortex is destroyed early in the eject phase, as seen in Fig. 5. This strong vortex is a chief source of the wall shear stress and flow stagnation in the center of the device, and may play an important role in thrombus formation. Strong rotating flow during filling was also observed experimentally in [62] and will be of interest in the future validation efforts.

Figures 6 and 7 show the time history of volume-averaged pressure and flow speed. The pressure drop across the membrane is small relative to the mean pressure, which is not surprising as it takes little effort to move the membrane. The peak average flow speed in the blood chamber during the fill stage is nearly 20 % greater than during the eject stage. Although the eject stage imposes a flow rate 50 % higher than the fill stage, the corresponding peak average flow speed is lower. This is in large part due to the rotational flow seen in Fig. 5, which is present only during the fill stage.

4 Conclusions and future work

This paper addressed several computational challenges involved in the FSI modeling of pulsatile VADs. These include large, buckling motions of the membrane, the need for periodic remeshing of the fluid mechanics domain, and the necessity to employ tightly coupled FSI solution strategies due to the very strong added mass effect present in the problem. Structural modeling of the membrane makes use of IGA, which has several accuracy and robustness benefits associated with the smoothness of the underlying discretization. The strong FSI coupling is efficiently implemented using a combination of matrix-free and sparse-matrix-based techniques. The simulations captured the essential blood flow features and structural deformations observed clinically and experimentally in pulsatile VADs. This is the first 3D, full-scale, high-fidelity FSI modeling of pulsatile VADs.

The computational FSI tools developed here provide a foundation for the study of the fluid and structural mechanics inside pulsatile VADs, with clinically relevant implications.

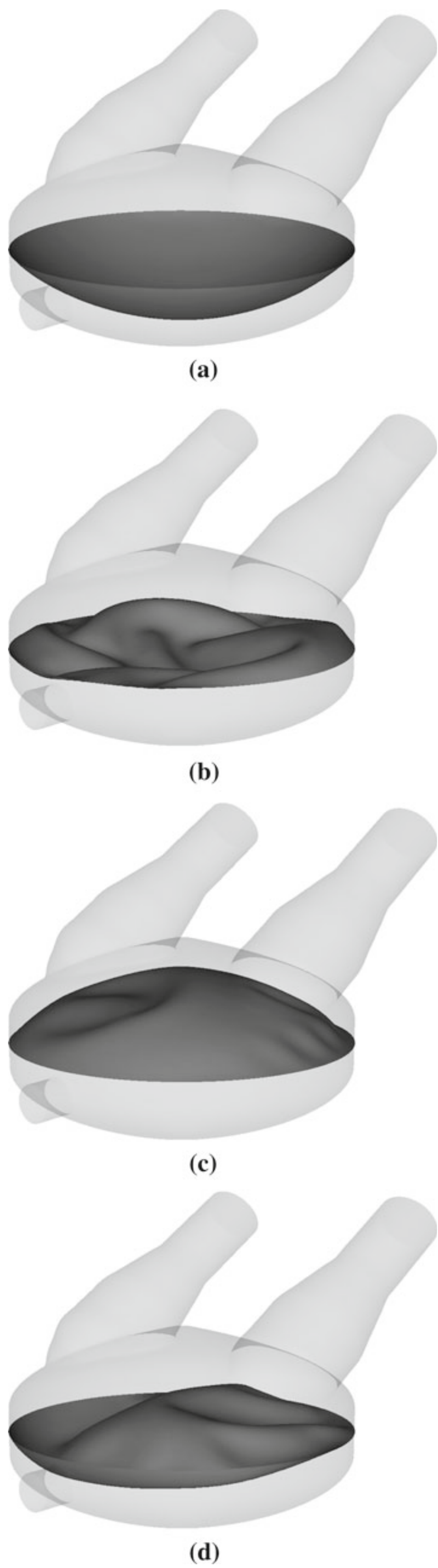

Fig. 4 The membrane deformed configuration at time **a** $t = 0$ s, **b** $t = 0.15$ s, **c** $t = 0.3$ s, and **d** $t = 0.525$ s

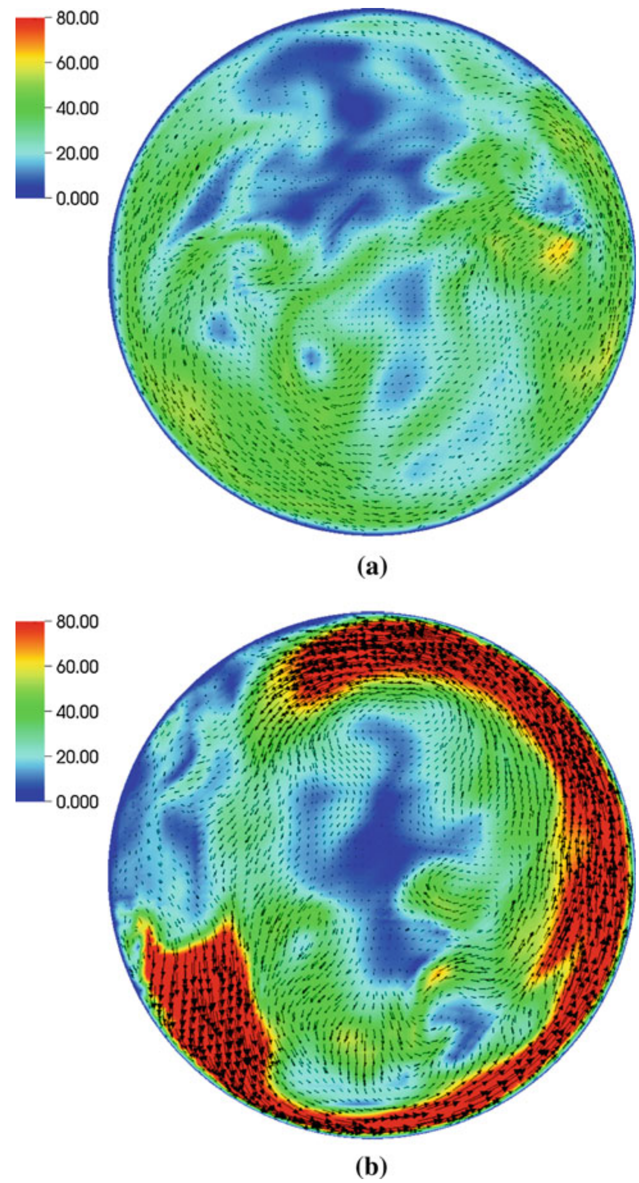

Fig. 5 Blood flow speed (cm/s) at 0.5 cm above the plane separating the blood and air chambers. In-plane vectors shown during (a) expel stage ($t = 0.14$ s) and (b) fill stage ($t = 0.665$ s)

We intend to use such simulations in the future to investigate design improvements that will mitigate risk of thrombosis, especially for pediatric populations. Methodically exploring a parameterized design space using computational FSI combined with modern optimization techniques and uncertainty quantification [54,55,64,66,103] may lead to novel designs that will improve patient outcomes. Thrombus formation involves a complex interplay between hemodynamics and blood chemistry, presenting significant modeling challenges [101,102]. Future work could incorporate reduced order models of blood chemistry to capture the key features of this process.

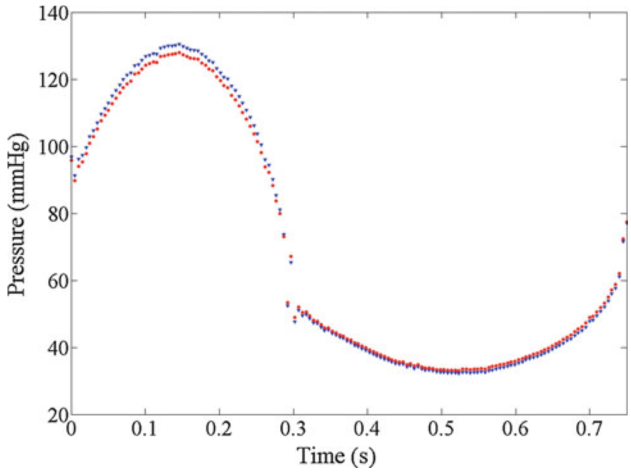

Fig. 6 Time history of the volume-averaged pressure in the blood and air chambers

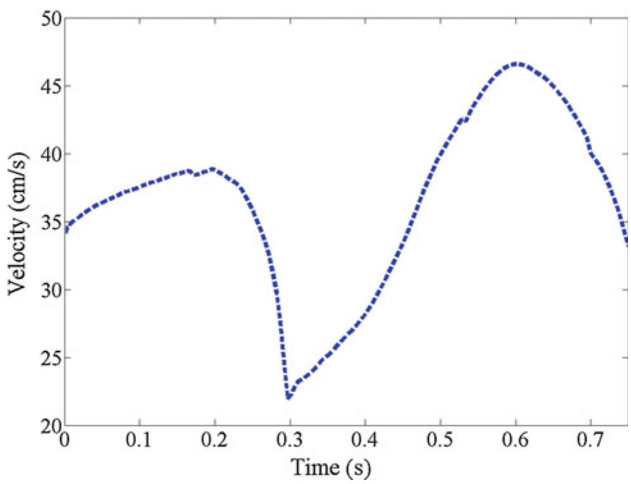

Fig. 7 Time history of the volume-averaged flow speed in the blood chamber

A strong validation effort is also planned. Particle Image Velocimetry data is available for the Penn State device [62], which we intend to simulate in the future.

Acknowledgments The support of the AFOSR Award No. FA9550-12-1-0005 and a Burroughs Wellcome Fund Career Award at the Scientific Interface is gratefully acknowledged. We also thank the San Diego Supercomputing Center (SDSC) at the University of California, San Diego for providing HPC resources that have contributed to the research results reported in this paper.

References

1. Akkerman I, Bazilevs Y, Benson DJ, Farthing MW, Kees CE (2012) Free-surface flow and fluid-object interaction modeling with emphasis on ship hydrodynamics. J Appl Mech 79:010905
2. Akkerman I, Bazilevs Y, Kees CE, Farthing MW (2011) Isogeometric analysis of free-surface flow. J Comput Phys 230:4137–4152
3. Akkerman I, Dunaway J, Kvandal J, Spinks J, Bazilevs Y (2012) Toward free-surface modeling of planing vessels: simulation of the Fridsma hull using ALE-VMS. Comput Mech 50:719–727
4. Amodeo A, Brancaccio G, Michielon G, Filippelli S, Ricci Z, Morelli S, Gagliardi MG, Iacobelli R, Pongiglione G, Di Donato RM (November 2010) Pneumatic pulsatile ventricular assist device as a bridge to heart transplantation in pediatric patients. Artif Organs 34(11):1017–1022
5. Arabia FA, Tsau PH, Smith RG, Nolan PE, Paramesh V, Bose RK, Woolley DS, Sethi GK, Rhenman BE, Copeland J (2006) Pediatric bridge to heart transplantation: application of the berlin heart, medos, and the thoratec ventricular assist devices. J Heart Lung Transplant 25(1):16–21
6. Bazilevs Y, Akkerman I (2010) Large eddy simulation of turbulent Taylor-Couette flow using isogeometric analysis and the residual-based variational multiscale method. J Comput Phys 229:3402–3414
7. Bazilevs Y, Calo VM, Cottrel JA, Hughes TJR, Reali A, Scovazzi G (2007) Variational multiscale residual-based turbulence modeling for large eddy simulation of incompressible flows. Comput Methods Appl Mech Eng 197:173–201
8. Bazilevs Y, Calo VM, Cottrell JA, Evans JA, Hughes TJR, Lipton S, Scott MA, Sederberg TW (2010) Isogeometric analysis using T-splines. Comput Methods Appl Mech Eng 199:229–263
9. Bazilevs Y, Calo VM, Hughes TJR, Zhang Y (2008) Isogeometric fluid-structure interaction: theory, algorithms, and computations. Comput Mech 43:3–37
10. Bazilevs Y, Hsu M-C, Benson D, Sankaran S, Marsden A (2009) Computational fluid-structure interaction: methods and application to a total cavopulmonary connection. Comput Mech 45: 77–89
11. Bazilevs Y, Hsu M-C, Kiendl J, Benson DJ (2012) A computational procedure for prebending of wind turbine blades. Int J Numer Methods Eng 89:323–336
12. Bazilevs Y, Hsu M-C, Kiendl J, Wüchner R, Bletzinger K-U (2011) 3D simulation of wind turbine rotors at full scale. Part II: Fluid-structure interaction modeling with composite blades. Int J Numer Methods Fluids 65:236–253
13. Bazilevs Y, Hsu M-C, Scott MA (2012) Isogeometric fluid-structure interaction analysis with emphasis on non-matching discretizations, and with application to wind turbines. Comput Methods Appl Mech Eng. doi:10.1016/j.cma.2012.03.028
14. Bazilevs Y, Ming-Chen H, Takizawa K, Tezduyar TE (2012) ALE-VMS and ST-VMS methods for computer modeling of wind-turbine rotor aerodynamics and fluid-structure interaction. Math Models Methods Appl Sci 22(supp 02):1230002
15. Bazilevs Y, Hughes TJR (2007) Weak imposition of Dirichlet boundary conditions in fluid mechanics. Comput Fluids 36: 12–26
16. Bazilevs Y, Michler C, Calo VM, Hughes TJR (2007) Weak Dirichlet boundary conditions for wall-bounded turbulent flows. Comput Methods Appl Mech Eng 196:4853–4862
17. Bazilevs Y, Michler C, Calo VM, Hughes TJR (2010) Isogeometric variational multiscale modeling of wall-bounded turbulent flows with weakly enforced boundary conditions on unstretched meshes. Comput Methods Appl Mech Eng 199:780–790
18. Bazilevs Y, Takizawa K, Tezduyar TE (2013) Computational fluid-structure interaction: methods and applications. Wiley, Chichester
19. Benson DJ, Bazilevs Y, De Luycker E, Hsu M-C, Scott M, Hughes TJR, Belytschko T (2010) A generalized finite element formulation for arbitrary basis functions: from isogeometric analysis to XFEM. Int J Numer Methods Eng 83:765–785
20. Benson DJ, Bazilevs Y, Hsu M-C, Hughes TJR (2010) Isogeometric shell analysis: the Reissner-Mindlin shell. Comput Methods Appl Mech Eng 199:276–289

21. Benson DJ, Bazilevs Y, Hsu M-C, Hughes TJR (2011) A large deformation, rotation-free, isogeometric shell. Comput Methods Appl Mech Eng 200:1367–1378
22. Brooks AN, Hughes TJR (1982) Streamline upwind/Petrov-Galerkin formulations for convection dominated flows with particular emphasis on the incompressible Navier-Stokes equations. Comput Methods Appl Mech Eng 32:199–259
23. Cavanaugh JL, Miyamoto SD, da Cruz E, Pietra BA, Campbell DN, Mitchell MB, Peyton CE, Gruenwald J, Darst JR (2010) Predicting recovery: successful explant of a ventricular assist device in a child with dilated cardiomyopathy. J Heart Lung Transplant 29(1):105–108
24. Chung J, Hulbert GM (1993) A time integration algorithm for structural dynamics withimproved numerical dissipation: the generalized-α method. J Appl Mech 60:371–375
25. Cirak F, Ortiz M (2001) Fully C^1-conforming subdivision elements for finite deformation thin shell analysis. Int J Numer Methods Eng 51:813–833
26. Cirak F, Ortiz M, Schröder P (2000) Subdivision surfaces: a new paradigm for thin shell analysis. Int J Numer Methods Eng 47:2039–2072
27. Cirak F, Scott MJ, Antonsson EK, Ortiz M, Schröder P (2002) Integrated modeling, finite-element analysis, and engineering design for thin-shell structures using subdivision. Computer-Aided Des 34:137–148
28. Dörfel MR, Jüttler B, Simeon B (2010) Adaptive isogeometric analysis by local h-refinement with T-splines. Comput Methods Appl Mech Eng 199:264–275
29. Haut Donahue TL, Dehlin W, Gillespie J, Weiss WJ, Rosenberg G (2009) Finite element analysis of stresses developed in the blood sac of a left ventricular assist device. Med Eng Phys 31: 454–460
30. Doyle MG, Vergniaud J-B, Tavoularis S, Bourgault Y (2008) Numerical simulations of blood flow in artificial and natural hearts with fluid-structure interaction. Artif Organs 32(11):870–879
31. Esmaily-Moghadam M, Migliavacca F, Vignon-Clementel IE, Hsia TY, Marsden AL (2012) Optimization of shunt placement for the norwood surgery using multi-domain modeling. J Biomed Eng 134: 5
32. Farhat C, Lesoinne M, Le Tallec P (1998) Load and motion transfer algorithms for fluid/structure interaction problems with non-matching discrete interfaces: momentum and energy conservation, optimal discretization and application to aeroelasticity. Comput Methods Appl Mech Eng 157:95–114
33. Hetzer R, Potapov EV, Stiller B et al (2006) Improvement in survival after mechanical circulatory support with pneumatic ventricula assist devices in pediatric patients. Annals Thorac Surg 82:917–925
34. Hsu M-C, Akkerman I, Bazilevs Y (2012) Wind turbine aerodynamics using ALE-VMS: validation and the role of weakly enforced boundary conditions. Comput Mech. doi:10.1007/s00466-012-0686-x
35. Hsu M-C, Akkerman I, Bazilevs Y (2013) Finite element simulation of wind turbine aerodynamics: validation study using NREL Phase VI experiment. Wind Energy. doi:10.1002/we.1599
36. Hsu M-C, Bazilevs Y (2012) Fluid-structure interaction modeling of wind turbines: simulating the full machine. Comput Mech 50:821–833
37. Hsu M-C, Bazilevs Y, Calo VM, Tezduyar TE, Hughes TJR (2010) Improving stability of stabilized and multiscale formulations in flow simulations at small time steps. Comput Methods Appl Mech Eng 199:828–840
38. Hughes TJR (1995) Multiscale phenomena: Green's functions, the Dirichlet-to-Neumann formulation, subgrid scale models, bubbles, and the origins of stabilized methods. Comput Methods Appl Mech Eng 127:387–401
39. Hughes TJR, Franca LP, Balestra M (1986) A new finite element formulation for computational fluid dynamics: V. Circumventing the Babuška-Brezzi condition: A stable Petrov-Galerkin formulation of the Stokes problem accommodating equal-order interpolations. Comput Methods Appl Mech Eng 59:85–99
40. Hughes TJR, Liu WK, Zimmermann TK (1981) Lagrangian-Eulerian finite element formulation for incompressible viscous flows. Comput Methods Appl Mech Eng 29:329–349
41. Hughes TJR, Sangalli G (2007) Variational multiscale analysis: the fine-scale Green's function, projection, optimization, localization, and stabilized methods. SIAM J Numer Anal 45:539–557
42. Hughes TJR, Scovazzi G, Franca LP (2004) Multiscale and stabilized methods. In: Stein E, de Borst R, Hughes TJR (eds) Encyclopedia of Computational Mechanics, vol. 3, Fluids chapter 2. Wiley, New York
43. Hughes TJR, Tezduyar TE (1984) Finite element methods for first-order hyperbolic systems with particular emphasis on the compressible Euler equations. Comput Methods Appl Mech Eng 45:217–284
44. Jansen KE, Whiting CH, Hulbert GM (2000) A generalized-α method for integrating the filtered Navier-Stokes equations with a stabilized finite element method. Comput Methods Appl Mech Eng 190:305–319
45. Johnson AA, Tezduyar TE (1994) Mesh update strategies in parallel finite element computations of flow problems with moving boundaries and interfaces. Comput Methods Appl Mech Eng 119:73–94
46. Johnson AA, Tezduyar TE (1996) Simulation of multiple spheres falling in a liquid-filled tube. Comput Methods Appl Mech Eng 134:351–373
47. Kalro V, Tezduyar TE (2000) A parallel 3D computational method for fluid-structure interactions in parachute systems. Comput Methods Appl Mech Eng 190:321–332
48. Kiendl J, Bazilevs Y, Hsu M-C, Wüchner R, Bletzinger K-U (2010) The bending strip method for isogeometric analysis of Kirchhoff-Love shell structures comprised of multiple patches. Comput Methods Appl Mech Eng 199:2403–2416
49. Kiendl J, Bletzinger K-U, Linhard J, Wüchner R (2009) Isogeometric shell analysis with Kirchhoff-Love elements. Comput Methods Appl Mech Eng 198:3902–3914
50. Konig CS, Clark C, Mokhtarzadeh-Dehghan MR (1999) Investigation of unsteady flow in a model of a ventricular assist device by numerical modeling and comparison with experiment. Mech Eng Phys 21(1):53–64
51. Kuttler U, Forster C, Wall WA (2006) A solution for the incompressibility dilemma in partitioned fluid-structure interaction with pure Dirichlet fluid domains. Comput Mech 38:417–429
52. Long CC, Hsu M-C, Bazilevs Y, Feinstein JA, Marsden AL (2012) Fluid-structure interaction simulations of the Fontan procedure using variable wall properties. Int J Numer Methods Biomed Eng 28:512–527
53. Marsden AL, Bernstein AD, Reddy VM, Shadden S, Spilker R, Chan FP, Taylor CA, Feinstein JA (2008) Evaluation of a novel Y-shaped extracardiac fontan baffle using computational fluid dynamics. J Thorac Cardiovasc Surg. doi:10.1016/j.jtcvs.2008.06.043
54. Marsden AL, Feinstein JA, Taylor CA (2008) A computational framework for derivative-free optimization of cardiovascular geometries. Comput Methods Appl Mech Eng 197(21–24):1890–1905
55. Marsden AL, Wang M, Dennis JE Jr, Moin P (2007) Trailing-edge noise reduction using derivative-free optimization and large-eddy simulation. J Fluid Mech 572:13–36
56. Mittal S, Tezduyar TE (1995) Parallel finite element simulation of 3D incompressible flows—Fluid-structure interactions. Int J Numer Methods Fluids 21:933–953

57. Nguyen-Thanh N, Kiendl J, Nguyen-Xuan H, Wüchner R, Bletzinger KU, Bazilevs Y, Rabczuk T (2011) Rotation-free isogeometric thin shell analysis using PHT-splines. Comput Methods Appl Mech Eng 200:3410–3424
58. Nordbeck S, Rystedt B (1967) Computer cartography point-in-polygon programs. BIT Numer Math 7:39–64
59. Oñate E, Flores FG (2005) Advances in the formulation of the rotation-free basic shell triangle. Comput Methods Appl Mech Eng 194:2406–2443
60. Oñate E, Zarate F (2000) Rotation-free triangular plate and shell elements. Int J Numer Methods Eng 47:557–603
61. Piegl L, Tiller W (1997) The NURBS book (monographs in visual communication), 2nd edn. Springer, Berlin
62. Roszelle BN, Deutsch S, Weiss WJ, Manning KB (2011) Flow visualization of a pediatric ventricular assist device during stroke volume reductions related to weaning. J Biomech Eng 39(7):2046–2058
63. Saad Y, Schultz M (1986) GMRES: a generalized minimal residual algorithm for solving nonsymmetric linear systems. SIAM J Sci Stat Comput 7:856–869
64. Sankaran S, Audet C, Marsden AL (2010) A method for stochastic constrained optimization using derivative-free surrogate pattern search and collocation. J Comput Phys 229(12):4664–4682
65. Sankaran S, Esmaily-Moghadam M, Kahn AM, Guccione J, Tseng E, Marsden AL (2012) Patient-specific multiscale modeling of blood flow for coronary artery bypass graft surgery. Annals Biomed Eng 40(1):2228–2242
66. Sankaran S, Marsden AL (2011) A stochastic collocation method for uncertainty quantification in cardiovascular simulations. J Biomech Eng 133(3):031001
67. San Diego Supercomputing Center (SDSC). http://www.sdsc.edu/. Accessed 15 April 2013
68. Sengupta D, Kahn AM, Burns JC, Sankaran S, Shadden S, Marsden AL (2012) Image-based modeling of hemodynamics and coronary artery aneurysms caused by kawasaki disease. Biomech Model Mechanobiol 11(6):915–932
69. Takizawa K, Bazilevs Y, Tezduyar TE (2012) Space-time and ALE-VMS techniques for patient-specific cardiovascular fluid-structure interaction modeling. Arch Comput Methods Eng 19:171–225
70. Takizawa K, Brummer T, Tezduyar TE, Chen PR (2012) A comparative study based on patient-specific fluid-structure interaction modeling of cerebral aneurysms. J Appl Mech 79:010908
71. Takizawa K, Christopher J, Tezduyar TE, Sathe S (2010) Space-time finite element computation of arterial fluid-structure interactions with patient-specific data. Int J Numer Methods Biomed Eng 26:101–116
72. Takizawa K, Moorman C, Wright S, Christopher J, Tezduyar TE (2010) Wall shear stress calculations in space-time finite element computation of arterial fluid-structure interactions. Comput Mech 46:31–41
73. Takizawa K, Moorman C, Wright S, Purdue J, McPhail T, Chen PR, Warren J, Tezduyar TE (2011) Patient-specific arterial fluid-structure interaction modeling of cerebral aneurysms. Int J Numer Methods Fluids 65:308–323
74. Takizawa K, Tezduyar TE (2011) Multiscale space-time fluid-structure interaction techniques. Comput Mech 48:247–267
75. Takizawa K, Tezduyar TE (2012) Computational methods for parachute fluid-structure interactions. Arch Comput Methods Eng 19:125–169
76. Takizawa K, Tezduyar TE (2012) Space-time fluid-structure interaction methods. Math Models Methods Appl Sci. doi:10.1142/S0218202512300013
77. Tezduyar T, Aliabadi S, Behr M, Johnson A, Mittal S (1993) Parallel finite-element computation of 3D flows. Computer 26(10):27–36
78. Tezduyar TE (1992) Stabilized finite element formulations for incompressible flow computations. Adv Appl Mech 28:1–44
79. Tezduyar TE (2001) Finite element methods for flow problems with moving boundaries and interfaces. Arch Comput Methods Eng 8:83–130
80. Tezduyar TE (2003) Computation of moving boundaries and interfaces and stabilization parameters. Int J Numer Methods Fluids 43:555–575
81. Tezduyar TE (2007) Finite elements in fluids: special methods and enhanced solution techniques. Comput Fluids 36:207–223
82. Tezduyar TE, Behr M, Liou J (1992) A new strategy for finite element computations involving moving boundaries and interfaces—the deforming-spatial-domain/space-time procedure: I. The concept and the preliminary numerical tests. Comput Methods Appl Mech Eng 94(3):339–351
83. Tezduyar TE, Behr M, Mittal S, Johnson AA (1992) Computation of unsteady incompressible flows with the finite element methods — space-time formulations, iterative strategies and massively parallel implementations. In: New methods in transient analysis PVP-vol. 246/AMD-vol. 143, pp 7–24, ASME, New York
84. Tezduyar TE, Behr M, Mittal S, Liou J (1992) A new strategy for finite element computations involving moving boundaries and interfaces—the deforming-spatial-domain/space-time procedure: II. Computation of free-surface flows, two-liquid flows, and flows with drifting cylinders. Comput Methods Appl Mech Eng 94(3):353–371
85. Tezduyar TE, Mittal S, Ray SE, Shih R (1992) Incompressible flow computations with stabilized bilinear and linear equal-order-interpolation velocity-pressure elements. Comput Methods Appl Mech Eng 95:221–242
86. Tezduyar TE, Osawa Y (2000) Finite element stabilization parameters computed from element matrices and vectors. Comput Methods Appl Mech Eng 190:411–430
87. Tezduyar TE, Park YJ (1986) Discontinuity capturing finite element formulations for nonlinear convection-diffusion-reaction equations. Comput Methods Appl Mech Eng 59:307–325
88. Tezduyar TE, Sathe S (2007) Modeling of fluid-structure interactions with the space-time finite elements: solution techniques. Int J Numer Methods Fluids 54:855–900
89. Tezduyar TE, Sathe S, Cragin T, Nanna B, Conklin BS, Pausewang J, Schwaab M (2007) Modeling of fluid-structure interactions with the space-time finite elements: arterial fluid mechanics. Int J Numer Methods Fluids 54:901–922
90. Tezduyar TE, Sathe S, Keedy R, Stein K (2004) Space-time techniques for finite element computation of flows with moving boundaries and interfaces. In: Gallegos S, Herrera I, Botello S, Zarate F, Ayala G (eds) Proceedings of the III International Congress on Numerical Methods in Engineering and Applied Science. CD-ROM, Monterrey, Mexico
91. Tezduyar TE, Sathe S, Keedy R, Stein K (2006) Space-time finite element techniques for computation of fluid-structure interactions. Comput Methods Appl Mech Eng 195:2002–2027
92. Tezduyar TE, Sathe S, Pausewang J, Schwaab M, Christopher J, Crabtree J (2008) Interface projection techniques for fluid-structure interaction modeling with moving-mesh methods. Comput Mech 43:39–49
93. Tezduyar TE, Sathe S, Schwaab M, Conklin BS (2008) Arterial fluid mechanics modeling with the stabilized space-time fluid-structure interaction technique. Int J Numer Methods Fluids 57:601–629
94. Tezduyar TE, Sathe S, Stein K (2006) Solution techniques for the fully-discretized equations in computation of fluid-structure interactions with the space-time formulations. Comput Methods Appl Mech Eng 195:5743–5753

95. Tezduyar TE, Schwaab M, Sathe S (2009) Sequentially-coupled arterial fluid-structure interaction (SCAFSI) technique. Comput Methods Appl Mech Eng 198:3524–3533
96. Tezduyar TE, Takizawa K, Brummer T, Chen PR (2011) Space-time fluid-structure interaction modeling of patient-specific cerebral aneurysms. Int J Numer Methods Biomed Eng 27:1665–1710
97. Tezduyar TE, Takizawa K, Moorman C, Wright S, Christopher J (2010) Multiscale sequentially-coupled arterial FSI technique. Comput Mech 46:17–29
98. Tezduyar TE, Takizawa K, Moorman C, Wright S, Christopher J (2010) Space-time finite element computation of complex fluid-structure interactions. Int J Numer Methods Fluids 64:1201–1218
99. Torii R, Oshima M, Kobayashi T, Takagi K, Tezduyar TE (2006) Computer modeling of cardiovascular fluid-structure interactions with the deforming-spatial-domain/stabilized space-time formulation. Comput Methods Appl Mech Eng 195:1885–1895
100. Torii R, Oshima M, Kobayashi T, Takagi K, Tezduyar TE (2006) Fluid-structure interaction modeling of aneurysmal conditions with high and normal blood pressures. Comput Mech 38:482–490
101. Zhiliang X, Chen N, Malgorzata MK, Elliot DR, Mark A (2008) A multiscale model of thrombus development. J R Soc Interface 5:705–722
102. Zhiliang X, Chen N, Shadden SC, Marsden JE, Malgorzata MK, Elliot DR, Mark A (2009) Study of blood flow impact on growth of thrombi using a multiscale model. Soft Matter 5(4):769–779
103. Yang W, Feinstein JA, Marsden AL (2010) Constrained optimization of an idealized y-shaped baffle for the fontan surgery at rest and exercise. Comput Methods Appl Mech Eng 199:2135–2149